NANO LETTERS

pubs.acs.org/NanoLett Letter

Engineering a Self-Assembled Protein Cage for Targeted Dual Functionalization

Xiao Ma, Lun Yi, Jiani Li, Juncai Ma, Wei Li, Lingqin Wang, Chunxue Liu, Bo Li, Ning Deng, Wei Kang,* and Chuang Xue*

Cite This: *Nano Lett.* 2024, 24, 9237−9244 Read Online

ACCESS | Metrics & More | Article Recommendations | Supporting Information

ABSTRACT: Self-assembled protein cages are attractive scaffolds for organizing various proteins of interest (POIs) toward applications in synthetic biology and medical science. However, specifically attaching multiple POIs to a single protein cage remains challenging, resulting in diversity among the functionalized particles. Here, we present the engineering of a self-assembled protein cage, $_{DT}Mi3_{ST}$, capable of independently recruiting two different POIs using SpyCatcher (SC)/SpyTag (ST) and DogCatcher (DC)/DogTag (DT) chemistries, thereby reducing variability between assemblies. Using fluorescent proteins as models, we demonstrate controlled targeting of two different POIs onto $_{DT}Mi3_{ST}$ protein cages both in vitro and inside living cells. Furthermore, dual functionalization of the $_{DT}Mi3_{ST}$ protein cage with a membrane-targeting peptide and β-galactosidase resulted in the construction of membrane-bound enzyme assemblies in *Escherichia coli*, leading to a 69.6% enhancement in substrate utilization across the membrane. This versatile protein cage platform provides dual functional nanotools for biological and biomedical applications.

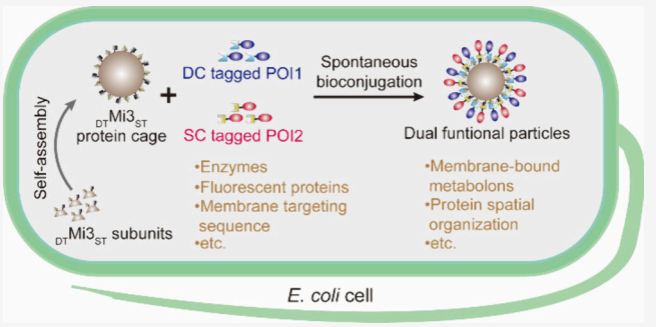

KEYWORDS: *self-assembled protein cage, protein scaffold, orthogonal bioconjugation, synthetic metabolon*

Self-assembled protein cages, such as ferritins, virus-like particles, encapsulins, and computationally designed protein cages, have caught extensive attention in the fields of bionanomaterials and synthetic biology.[1,2] These protein cages are self-assembled from multiple copies of a single (or a few) protein subunits, resulting in highly organized structures with well-defined interior and exterior surfaces. They feature unprecedented homogeneity, biocompatibility, and multiple modifiable sites, making them ideal scaffolds for organizing proteins of interest (POIs). One crucial aspect in the construction of protein cage scaffolded bionanomaterials is the functionalization of protein cages. Various strategies have been explored, including loading cargoes into the interior cavity or attaching them to the exterior surface of protein cages by chemical or genetic modification.[3−10] These functionalized protein cages have shown promise in applications such as drug/gene delivery,[11−13] enzymatic reactions,[6,14−18] vaccines/antigen presentation,[19−21] and the assembly of higher-order structures.[22,23]

However, while significant progress has been made in functionalizing protein cages, site-specifically functionalizing the cages with multiple different cargo proteins remains challenging, particularly for applications requiring diverse functionalities such as targeting sequences, fluorescent proteins, biocatalytic activities, and therapeutic agents. Many current studies rely on single bioconjugation strategies, and thus, cargo proteins may compete for the same attachment site, resulting in heterogeneous assemblies with varying numbers and stoichiometries of attached cargo proteins. Yet, the homogeneity of these assemblies is crucial for the fine-tuning of the biological activities of the functionalized protein cages. Thus, efforts have been directed toward engineering protein cages capable of orthogonally recruiting different POIs. In a previous study, an engineered protein cage derived from the cowpea chlorotic mottle virus (CCMV) capsid was demonstrated to have surface-exposed native cysteine and non-canonical amino acid azido-phenylalanine incorporated through the amber suppression.[24] This modification enabled the site-specific recruitment of two different cargo proteins using orthogonal chemical reactions, i.e., the maleimide reaction and "click" reaction. However, the necessity of performing chemical coupling reactions in vitro after purification of the protein cage hinders its suitability for in

Received: April 10, 2024
Revised: July 13, 2024
Accepted: July 15, 2024
Published: July 17, 2024

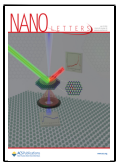

https://doi.org/10.1021/acs.nanolett.4c01693
Nano Lett. 2024, 24, 9237−9244

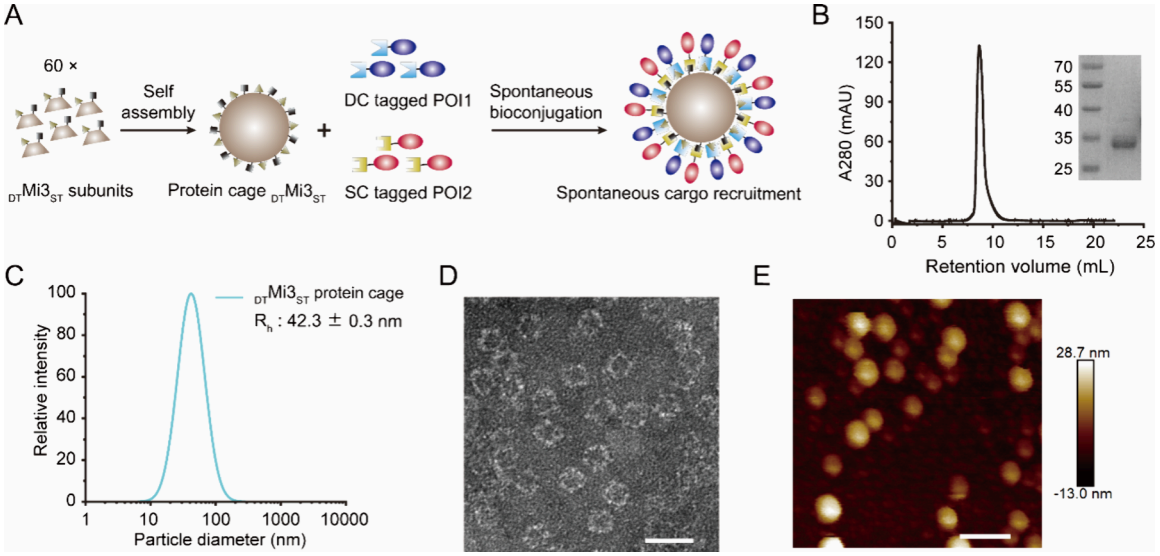

Figure 1. Design and construction of the $_{DT}Mi3_{ST}$ protein cage for spontaneous recruitment of DC/SC-tagged POIs. (A) Schematic representation of engineering the $_{DT}Mi3_{ST}$ protein cage platform. (B) SEC and SDS-PAGE analysis of the purified $_{DT}Mi3_{ST}$ protein cage. (C) DLS determination of the hydrodynamic radius (R_h) of $_{DT}Mi3_{ST}$. The result is presented in a log-normal distribution. (D) Negatively stained TEM image of the $_{DT}Mi3_{ST}$ protein cages. Scale bar: 50 nm. (E) AFM image of $_{DT}Mi3_{ST}$ protein cages. Color bar on the right indicates the height of the structures. Scale bar: 100 nm.

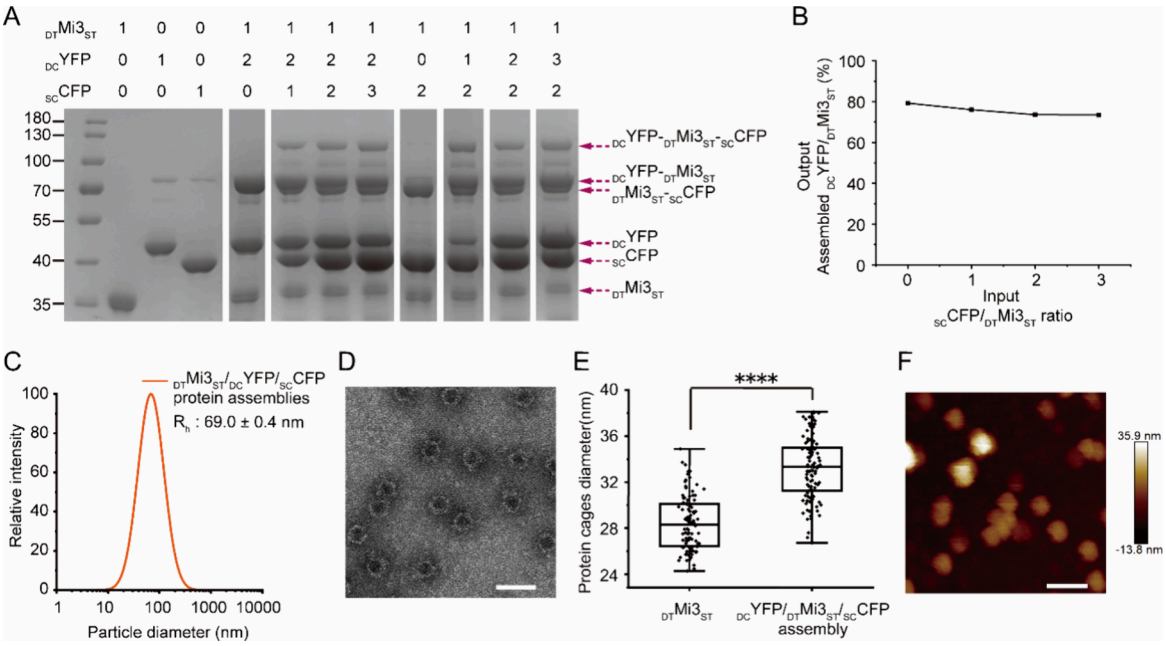

Figure 2. $_{DT}Mi3_{ST}$ scaffolded assembly of fluorescent proteins in test tubes. (A) SDS-PAGE analysis of protein mixtures consisting of $_{DC}YFP$, $_{DT}Mi3_{ST}$, and $_{SC}CFP$. The molar ratio of different proteins is indicated at the top of the gel image. Bands with higher molecular weight indicate the orthogonal and covalent conjugation between the $_{DT}Mi3_{ST}$ protein cage and DC/SC-containing proteins. (B) Quantification of data in lines 5−8 in A revealing that the input $_{SC}CFP/_{DT}Mi3_{ST}$ ratio did not influence the conjugation efficiency between $_{DC}YFP$ and $_{DT}Mi3_{ST}$ (see Figure S4 for quantification of data in lines 9−12 in A). The output ratio was calculated as [band intensity(total $_{DC}YFP$) − band intensity(unconjugated $_{DC}YFP$)]/band intensity(total $_{DT}Mi3_{ST}$). (C) DLS analysis of the protein cage scaffolded assemblies, indicating the R_h of $_{DC}YFP/_{DT}Mi3_{ST}/_{SC}CFP$ assemblies. (D) Negatively stained TEM image of $_{DC}YFP/_{DT}Mi3_{ST}/_{SC}CFP$ assemblies. Scale bars: 50 nm. (E) Quantification and comparison of particle diameters of $_{DT}Mi3_{ST}$ protein cages and $_{DC}YFP/_{DT}Mi3_{ST}/_{SC}CFP$ assemblies (n = 100 for each group). Unpaired t test was performed (****: $P < 0.0001$). (F) AFM image of $_{DC}YFP/_{DT}Mi3_{ST}/_{SC}CFP$ assemblies. Color bar on the right indicates the height of the structures. Scale bar: 100 nm.

vivo applications. For in vivo dual site-specific functionalization of protein cages, orthogonal sortases are attractive. A previous study has demonstrated independent conjugation of various cargo moieties to the M13 phage particle by using sortases from different bacteria.[25] Nevertheless, this strategy relies on the coexpression of sortase in living cells for in vivo dual labeling, which may impose cellular burden or unintended biological effects on host cells.

Mi3 is a computationally designed dodecahedral protein cage based on an aldolase of thermophilic bacteria.[21] In our

https://doi.org/10.1021/acs.nanolett.4c01693
Nano Lett. 2024, 24, 9237−9244

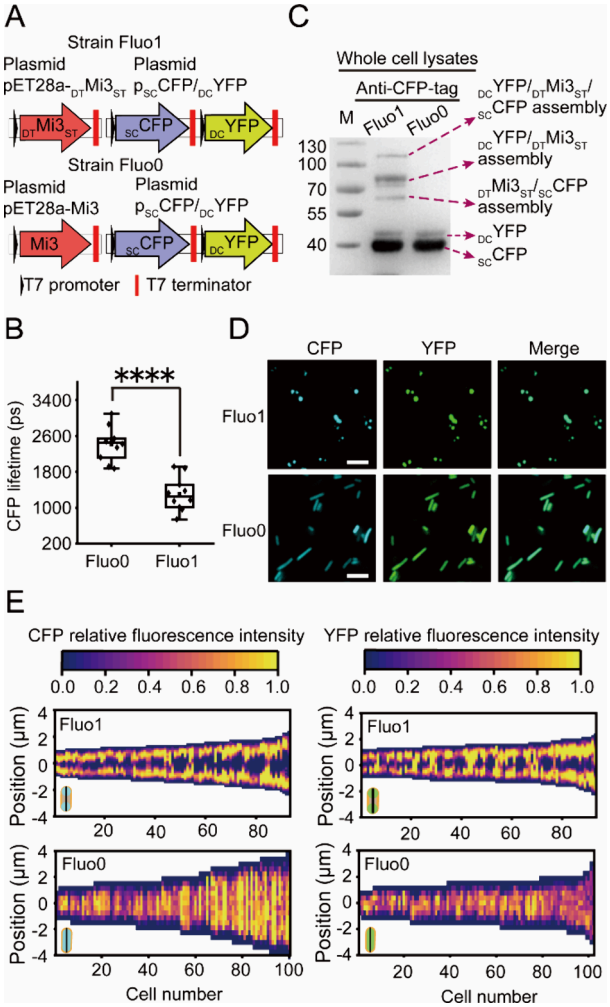

Figure 3. $_{DT}Mi3_{ST}$ scaffolded assemblies of fluorescent proteins in *E. coli*. (A) Genetic constructs for the expression of fluorescent proteins and Mi3 protein cages. Strain Fluo0 (control strain) expressing $_{SC}$CFP, $_{DC}$YFP, and the untagged Mi3 protein cage. Strain Fluo1 expressing $_{SC}$CFP, $_{DC}$YFP, and the $_{DT}Mi3_{ST}$ protein cage. (B) Measurement of the $_{SC}$CFP lifetime in engineered *E. coli* cells were obtained by fluorescence lifetime imaging microscopy. $_{SC}$CFP exhibits a decreased lifetime in Fluo1 due to the fluorescence resonance energy transfer (FRET) resulting from the $_{DT}Mi3_{ST}$-mediated colocalization of $_{SC}$CFP and $_{DC}$YFP. Significance was calculated by *t* test. ****$P < 0.0001$ ($n = 10$ cells for each group). (C) Western blot analysis of whole cell lysates showing covalent conjugation in Strain Fluo1. (D) Confocal images of the two engineered *E. coli* strains showing distinctive fluorescent signals. Scale bars: 5 μm. (E) Localization patterns of $_{SC}$CFP and $_{DC}$YFP shown in D were quantified. Vertical heatmaps representing intensities of fluorescent proteins across the long cell axis were generated using ImageJ. Demographs show the fluorescent intensity across a population of cells arranged by cell length. Uniform fluorescence was observed in Strain Fluo0. In contrast, fluorescence was concentrated at the poles of Fluo1.

previous work, we have successfully achieved functionalization of the Mi3 protein cage via the SpyCatcher/SpyTag system,[26] chemical-induced dimerization domains, or light-induced dimerization domains.[17] After a close examination of the structure, we found that both of its C- and N-termini are surface exposed (Figure S1), making it an ideal candidate for engineering a dual functionalizable nanoplatform. We chose to use recently developed SpyTag/SpyCatcher (ST/SC) and DogTag/DogCatcehr (DT/DC) systems to independently recruit DC- and SC-tagged cargo proteins via orthogonal chemistries. ST can form an irreversible isopeptide bond with SC upon mixing.[27] The DT/DC system is similar to the ST/SC system but orthogonal.[28] Our engineered protein cage offers several advantages, including the ability to perform dual functionalization not only in vitro but also in vivo, without the need for downstream chemical manipulation or introduction of external enzymes.

Here, we present the engineering of the Mi3 protein cage as a nanoplatform, termed $_{DT}Mi3_{ST}$, capable of independently recruiting two different cargo proteins via orthogonal isopeptide formation systems both in vitro and in living cells. Using fluorescent proteins as model cargoes, we demonstrate orthogonal attachment of different POIs to the exterior of the protein cage. By employing a membrane-targeting peptide and β-galactosidase as protein cargoes, we successfully construct membrane-bound protein assemblies based on the $_{DT}Mi3_{ST}$ protein cage, leading to an enhanced substrate utilization across the membrane. This advancement significantly expands the toolbox of dual-functional nanotools for a wide range of applications in synthetic biology and medical science.

To develop a protein cage platform that can orthogonally recruit two types of protein cargos, we chose to use the Mi3 protein cage along with ST/SC and DT/DC systems. For this, ST and DT were fused to the N- and C-terminus of the Mi3 subunit, generating a chimera, namely, $_{DT}Mi3_{ST}$ (Figure 1A).

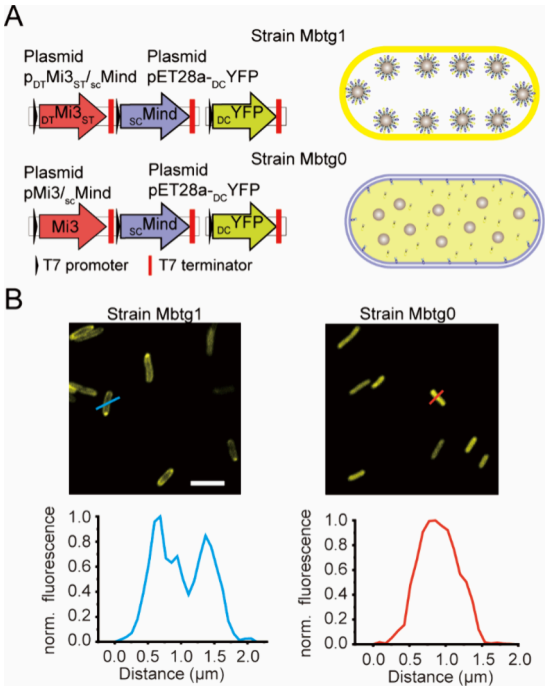

Figure 4. Characterization of $_{DT}Mi3_{ST}$ scaffolded membrane bound assemblies. (A) Schematic of genetic constructs for the expression of $_{DT}Mi3_{ST}$ protein cages and cargo proteins possessing different functions ($_{DC}$YFP and $_{SC}$MinD). Strain Mbtg0 (control strain) expressing $_{SC}$MinD, $_{DC}$YFP, and the naked Mi3 protein cage. Strain Mbtg1 expressing $_{SC}$MinD, $_{DC}$YFP, and the $_{DT}Mi3_{ST}$ protein cage. (B) Confocal images of the two engineered *E. coli* strains showing distinctive fluorescent signals. Dual functionalization of $_{DT}Mi3_{ST}$ allows for the precise spatial organization of YFP on the *E. coli* cell membrane (top panels). Scale bars: 5 μm. Bottom panels: Quantification of YFP signals along the line cuts.

https://doi.org/10.1021/acs.nanolett.4c01693
Nano Lett. 2024, 24, 9237−9244

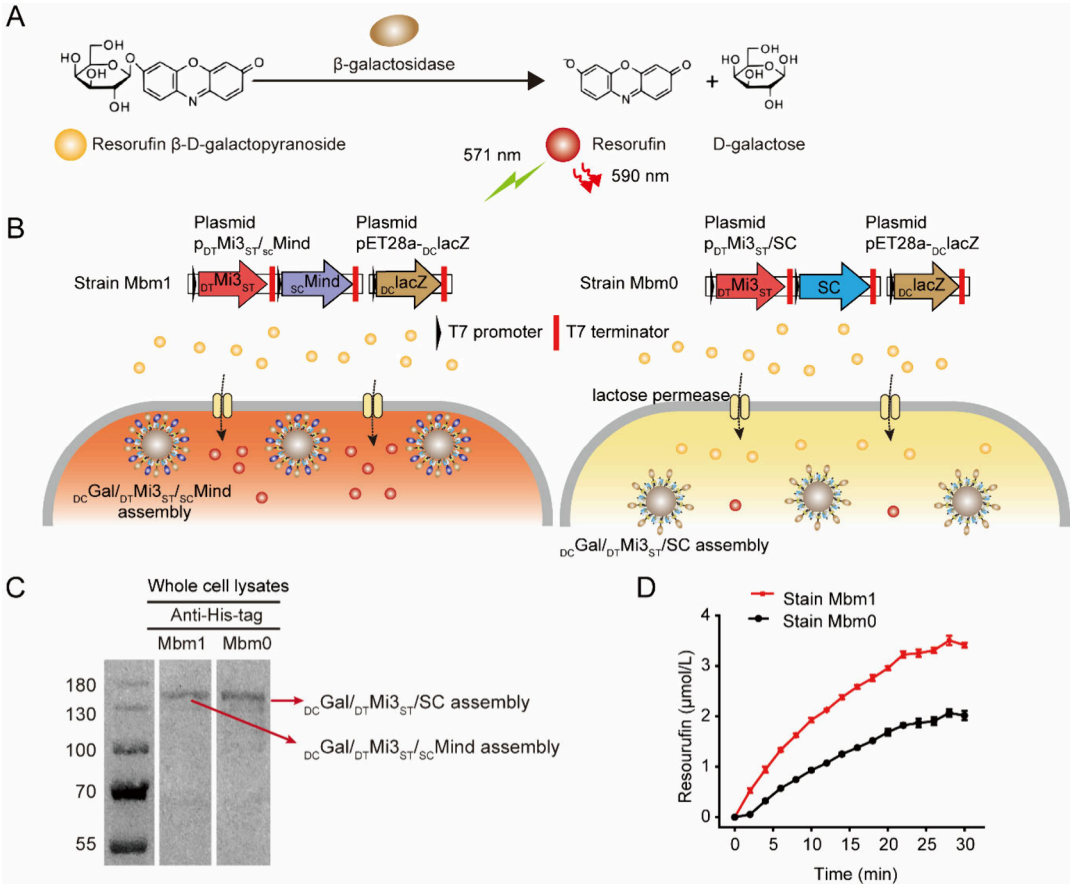

Figure 5. Enhanced substrate utilization by synthetic membrane-bound enzyme assemblies. (A) Hydrolysis of resorufin *β*-D-galactopyranoside by *β*-galactosidase generates D-galactose and resorufin. (B) Schematic of engineered strains with synthetic metabolons. Strain Mbm1 expressing $_{DT}Mi3_{ST}$, $_{SC}$MinD, and $_{DC}$Gal. Strain Mbm0 (control strain) expressed $_{DT}Mi3_{ST}$, SC, and $_{DC}$Gal. Top panels: Genetic constructs for Strains Mbm1 and Mbm0. Bottom panels: Enhanced substrate utilization by membrane-bound enzyme assemblies in Strain Mbm1. (C) Western blot analysis of whole cell lysates showing the covalent conjugation between the $_{DT}Mi3_{ST}$ protein cage and POIs. Mbm1 expressing the $_{DT}Mi3_{ST}$ protein cage, $_{DC}$Gal, and $_{SC}$MinD; Mbm0 expressing the $_{DT}Mi3_{ST}$ protein cage, $_{DC}$Gal, and SC. (D) Comparison of resorufin titers between the two engineered strains showing enhanced resorufin biosynthesis in Strain Mbm1.

To avoid steric hindrance, flexible linkers were inserted between the DT/ST and Mi3. We first purified and characterized the engineered proteins. 6×His-tagged $_{DT}Mi3_{ST}$ was expressed in *E. coli* and purified to homogeneity using metal-affinity chromatography (IMAC). Then, the purified protein was analyzed by size exclusion chromatography (SEC). $_{DT}Mi3_{ST}$ particles eluted as a single peak at the void volume. SDS-PAGE analysis of the collected peak showed a single band corresponding to the $_{DT}Mi3_{ST}$ subunit (29.6 kDa) (Figure 1B). These results demonstrated that $_{DT}Mi3_{ST}$ was expressed in the soluble form and self-assembled into particles with a higher molecular weight exceeding the upper limit of SEC. To investigate the morphology of $_{DT}Mi3_{ST}$ particles, $_{DT}Mi3_{ST}$ was further characterized using dynamic light scattering (DLS), transmission electron microscope (TEM), and atomic force microscope (AFM). DLS analysis of $_{DT}Mi3_{ST}$ gave a uniform peak with a hydrodynamic radius (R_h) of 42.3 ± 0.3 nm (Figure 1C). Moreover, TEM and AFM images showed that $_{DT}Mi3_{ST}$ particles exhibit intact, homogeneous, and cage-like structures (Figure 1D,E). Additionally, the resultant protein cage remained stable under physiological conditions after incubation at room temperature for 72 h (Figure S2). Altogether, these results demonstrated that chimeric $_{DT}Mi3_{ST}$ can readily self-assemble into protein cages.

Next, we investigated whether the $_{DT}Mi3_{ST}$ protein cage can recruit proteins containing the cognate interaction proteins independently. We chose to use SC-tagged cyan fluorescent protein ($_{SC}$CFP, 39.1 kDa) and DC-tagged yellow fluorescent protein ($_{DC}$YFP, 41.3 kDa) as model proteins. To this end, $_{SC}$CFP and $_{DC}$YFP were expressed and purified to homogeneity (Figure S3), separately. Then, cargo proteins of $_{SC}$CFP and $_{DC}$YFP were mixed with $_{DT}Mi3_{ST}$ protein cages at indicated molar ratios in 50 mM Tris buffer (pH 7.6) for 1 h at room temperature (Figure 2A). The SDS-PAGE analysis of protein mixtures showed extra bands with higher molecular weight at approximately 68.7 and 70.9 kDa, which correspond to the conjugated adducts (i.e., $_{DT}Mi3_{ST}/_{SC}$CFP assembly and $_{DC}$YFP/$_{DT}Mi3_{ST}$ assembly, respectively), indicating the covalent bond formation between $_{DT}Mi3_{ST}$ and POIs (Figure 2A). However, not all the attachment sites were occupied by client proteins, even in the excess amount of cargo proteins. This may be due to the inherent limitation of the coupling reactions and/or insufficient surface exposure of SpyTag/DogTag. Further study is needed to improve the bioconjugation efficiency, such as screening of optimal variants of SpyCatcher and DogCatcher[29] and optimizing the linker sequence between SpyTag/DogTag and the protein cage subunit. In addition, when both cargo proteins were mixed

https://doi.org/10.1021/acs.nanolett.4c01693
Nano Lett. 2024, 24, 9237−9244

with $_{DT}Mi3_{ST}$ particles, another band with a higher molecular weight (109.9 kDa) was also observed, which corresponds to $_{DT}Mi3_{ST}$ subunits conjugated with both $_{SC}$CFP and $_{DC}$YFP ($_{DC}$YFP/$_{DT}Mi3_{ST}$/$_{SC}$CFP assembly). The presence of the $_{DC}$YFP/$_{DT}Mi3_{ST}$/$_{SC}$CFP assembly demonstrated that both cargoes can be attached to the same protein cage simultaneously. Notably, densitometry analyses of the SDS-PAGE gel (Figure 2A) revealed that increasing the input $_{SC}$CFP/$_{DT}Mi3_{ST}$ ratio had no influence on the conjugation efficiency between $_{DC}$YFP and $_{DT}Mi3_{ST}$, and vice versa (Figure 2B and Figure S4), indicating orthogonal conjugation between the $_{DT}Mi3_{ST}$ protein cage and two types of POIs. Moreover, the ratio of DC-tagged POI and SC-tagged POI recruited by the protein cage can be regulated simply by altering the input ratio of DC-tagged POI and SC-tagged POI (Figure S5).

Then, protein cage scaffolded assemblies were purified by SEC (Figure S6) and subjected to further characterization using DLS, TEM, and AFM analyses. Specifically, DLS showed an increased R_h value of 69.0 ± 0.4 nm (Figure 2C), which was attributed to the successful assembly of fluorescent proteins. TEM images revealed that $_{DC}$YFP/$_{SC}$CFP attached protein cages exhibited intact and cage-like structures, but with blurred edges (Figure 2D). Additionally, the TEM images showed an increased diameter compared to naked $_{DT}Mi3_{ST}$ protein cages (28.6 ± 2.3 nm vs 33.3 ± 2.7 nm, Figure 2E). The increased particle size was corroborated by AFM images (Figure 2F), confirming the successful attachment of fluorescent proteins onto the surfaces of the $_{DT}Mi3_{ST}$ protein cages. Altogether, these results demonstrated that $_{DT}Mi3_{ST}$ protein cages successfully served as a nanoplatform for the recruitment of both SC-containing proteins and DC-containing proteins orthogonally.

After validating the covalent conjugation, we tested whether $_{DT}Mi3_{ST}$ particles can organize proteins in complex intracellular environments using the fluorescence resonance energy transfer (FRET) pair of CFP and YFP as model cargoes. To this end, plasmid encoding $_{SC}$CFP and $_{DC}$YFP and plasmid encoding $_{DT}Mi3_{ST}$ were co-transformed into *E. coli*, resulting in Strain Fluo1 (Figure 3A). Similarly, Strain Fluo0 expressing $_{SC}$CFP, $_{DC}$YFP, and untagged Mi3 was also created to serve as a control. Both strains were then examined by fluorescence lifetime imaging microscopy (FLIM). The fluorescence lifetime of $_{SC}$CFP (the donor of the CFP/YFP FRET pair) was significantly decreased in Strain Fluo1 compared to that in Fluo0 (1304.9 ps vs 2412.9 ps; Figure 3B) because of FRET, indicating the colocalization of $_{SC}$CFP and $_{DC}$YFP. The distance between the $_{SC}$CFP and $_{DC}$YFP was calculated to be 4.0 nm according to the FRET efficiency (see details in the Experimental Section), indicating the high density of assembled fluorescent proteins on the surface of $_{DT}Mi3_{ST}$. The spontaneous bioconjugation between $_{DT}Mi3_{ST}$ and fluorescent proteins in Strain Fluo1 was further confirmed by Western blot (Figure 3C and Figure S7). Specifically, Strain Fluo0 showed only bands of $_{DC}$YFP and $_{SC}$CFP, whereas in Strain Fluo1, extra bands corresponding to $_{DC}$YFP/$_{DT}Mi3_{ST}$ assembly, $_{DT}Mi3_{ST}$/$_{SC}$CFP assembly, and $_{DC}$YFP/$_{DT}Mi3_{ST}$/$_{SC}$CFP assembly were observed. Additionally, Strain Fluo0 exhibited a uniform distribution of both CFP and YFP signals throughout the entire cell. In contrast, Strain Fluo1 displayed signals concentrating at the poles of the cells (Figure 3D and 3E), possibly resulting from the exclusion of protein assemblies from the cell center by genomic DNA, which could be caused by the increased size of protein assemblies compared with that of "free" proteins. Intracellular protein cage scaffolded assemblies were morphologically analyzed using thin-section TEM, revealing intact and spherical particles with an increased average diameter compared to that of naked protein cages (99.0 nm vs 65.6 nm, Figure S8). Altogether, these results demonstrated that the $_{DT}Mi3_{ST}$ scaffolded protein assembly of DC/SC-containing proteins can be achieved in complex intracellular environments.

Due to the unique ability to selectively recruit both SC-containing and DC-containing cargoes, the $_{DT}Mi3_{ST}$ protein cage can be easily decorated with dual functionality by employing POIs possessing diverse functional characteristics. To this end, we employed the membrane-localizing region of MinD from *Bacillus subtilis* as an alternative cargo protein,[30,31] thereby conferring membrane-targeting capability to $_{DT}Mi3_{ST}$. Specifically, we genetically fused the membrane-targeting sequence to the C-terminal of SC, resulting in $_{SC}$MinD. Subsequently, the $_{DT}Mi3_{ST}$ protein cage, $_{SC}$MinD, and $_{DC}$YFP were coexpressed in *E. coli* (Strain Mbtg1) using two compatible plasmids (Figure 4A). A control strain (Strain Mbtg0) expressing the naked Mi3 protein cage, $_{SC}$MinD, and $_{DC}$YFP was also generated for comparison. As anticipated, two strains showed different fluorescent patterns, as examined under a fluorescent microscope. In Strain Mbtg0, $_{DC}$YFP displayed dispersed signals within the cytoplasm, whereas in Strain Mbtg1, the $_{DC}$YFP signal colocalized with the cell membrane (Figure 4B). This observation confirmed the spontaneous conjugation of the $_{DT}Mi3_{ST}$ protein cage with both $_{SC}$MinD and $_{DC}$YFP, which led to the formation of the $_{DC}$YFP/$_{DT}Mi3_{ST}$/$_{SC}$MinD assembly. Furthermore, the assembly was effectively targeted to the cell membrane of *E. coli* by $_{SC}$MinD, providing compelling evidence for the dual functionalization capability of the $_{DT}Mi3_{ST}$ protein cage and precise organization of proteins on the *E. coli* cell membrane.

The efficient utilization of substrates across biological membranes is a fundamental prerequisite for synthesizing chemical products in cellular factories. Membrane-bound metabolons, with significant potential to enhance substrate transportation efficiency and minimize diversion to competing pathways, have been developed to improve the biosynthesis efficiency. For example, an artificial transport metabolon has been created in yeast by constructing an artificial complex between an endogenous sugar transporter and a heterologous xylose isomerase, accelerating the utilization of xylose.[32] In contrast to reported approaches, we developed membrane-bound metabolons by dual functionalization of the $_{DT}Mi3_{ST}$ protein cage with both $_{SC}$MinD and DC targeted enzymes. As a proof of principle, we employed β-galactosidase, a glycoside exonuclease, which can convert nonfluorescent resorufin β-D-galactopyranoside (RDG) to a bright pink fluorescent product (Figure 5A), making it easy to quantitatively monitor reactions by spectrometric methods with a standard curve (Figure S9).[33]

To this end, $_{DT}Mi3_{ST}$, $_{SC}$MinD, and DC-containing β-galactosidase ($_{DC}$Gal) were coexpressed in LacZ-deficient *E. coli*, giving Strain Mbm1. A control strain expressing $_{DT}Mi3_{ST}$, SC, and $_{DC}$Gal was also constructed (Figure 5B). The covalent conjugation between $_{DT}Mi3_{ST}$ and cargoes in engineered strains was confirmed by Western blot (Figure 5C). Strikingly, Strain Mbm1 showed a 69.6% increase in resorufin signal compared with Strain Mbm0 (Figure 5D). We speculated that the formation of membrane-bound metabolons contributes to

https://doi.org/10.1021/acs.nanolett.4c01693
Nano Lett. 2024, 24, 9237−9244

the increase in resorufin production. Particularly, in Mbm1, the $_{DC}$Gal/$_{DT}$Mi3$_{ST}$/$_{SC}$MinD assemblies were targeted to the vicinity of membrane-associated lactose permeases, which served as the entrances of the RDG into *E. coli* cells, leading to the formation of membrane-bound metabolons (Figure 5B, left) capable of preventing substrate diversion away from $_{DC}$Gal, leading to an increase in resorufin production. In contrast, in Mbm0, the absence of MinD blocked the proximity of $_{DC}$Gal and lactose permeases, resulting in low levels of resorufin production. Besides, densitometry analysis of bands in Western blot showed a similar protein abundance of $_{DC}$Gal in two strains, excluding the impact of different protein expression levels on the reaction. It will be very interesting to further explore how factors such as the relative ratio, spacing, and orientation of the attached enzymes affect catalytic activities of the protein cage scaffolded assemblies. Overall, these results indicate that $_{DT}$Mi3$_{ST}$ can be used to construct membrane-bound metabolons in living cells and accelerate biosynthesis by facilitating substrate utilization.

In this work, we have developed a self-assembled protein cage, namely, $_{DT}$Mi3$_{ST}$, which can be dual functionalized by orthogonally recruiting two types of POIs containing cognate interaction domains. This strategy can avoid competition for the same binding site among different POIs, effectively reducing the variability among protein scaffolded assemblies. Using model fluorescent proteins, we demonstrated that two types of POIs can be attached to the surface of the $_{DT}$Mi3$_{ST}$ protein cage without interfering with each other, not only in vitro but also inside living cells. Furthermore, by recruiting a membrane-targeting sequence and β-galactosidase to the surface of the protein cage, we constructed membrane-bound metabolons within *E. coli* cells, leading to a 69.6% increase in RDG utilization across the membrane. We envision that the dual functionalization of the $_{DT}$Mi3$_{ST}$ protein cage with diverse POIs holds potential for applications in synthetic biology and medical science (e.g., development of effective, multivalent vaccines against communicable diseases by recruiting multiple antigens, enabling broadening of protection coverage and enhancement of immune response). In the context of the latter applications, further study is needed to investigate the effects of the engineered scaffolds on mammalian cells. This is particularly important for biomedical applications, such as delivering therapeutic agents.

■ ASSOCIATED CONTENT

Supporting Information

The Supporting Information is available free of charge at https://pubs.acs.org/doi/10.1021/acs.nanolett.4c01693.

Detailed experimental methods, details of DNA and protein sequences, characterization of protein expression and purification; additional figures (PDF)

■ AUTHOR INFORMATION

Corresponding Authors

Wei Kang − *State Key Laboratory of Fine Chemicals, Frontiers Science Centre for Smart Materials Oriented Chemical Engineering, School of Bioengineering, Dalian University of Technology, Dalian 116024, China; Ningbo Institute of Dalian University of Technology, Ningbo 315016, China;* Email: kangwei@dlut.edu.cn

Chuang Xue − *State Key Laboratory of Fine Chemicals, Frontiers Science Centre for Smart Materials Oriented Chemical Engineering, School of Bioengineering, Dalian University of Technology, Dalian 116024, China; Ningbo Institute of Dalian University of Technology, Ningbo 315016, China;* orcid.org/0000-0002-3856-8457; Email: xue.1@dlut.edu.cn

Authors

Xiao Ma − *State Key Laboratory of Fine Chemicals, Frontiers Science Centre for Smart Materials Oriented Chemical Engineering, School of Bioengineering, Dalian University of Technology, Dalian 116024, China; Ningbo Institute of Dalian University of Technology, Ningbo 315016, China;* orcid.org/0000-0003-2978-8500

Lun Yi − *State Key Laboratory of Fine Chemicals, Frontiers Science Centre for Smart Materials Oriented Chemical Engineering, School of Bioengineering, Dalian University of Technology, Dalian 116024, China; School of Chemistry and Biological Engineering, University of Science and Technology Beijing, Beijing 100083, China*

Jiani Li − *State Key Laboratory of Fine Chemicals, Frontiers Science Centre for Smart Materials Oriented Chemical Engineering, School of Bioengineering, Dalian University of Technology, Dalian 116024, China*

Juncai Ma − *School of Life Sciences, Centre for Cell & Developmental Biology and State Key Laboratory of Agrobiotechnology, The Chinese University of Hong Kong, Shatin, Hong Kong 999077, China*

Wei Li − *State Key Laboratory of Fine Chemicals, Frontiers Science Centre for Smart Materials Oriented Chemical Engineering, School of Bioengineering, Dalian University of Technology, Dalian 116024, China*

Lingqin Wang − *State Key Laboratory of Fine Chemicals, Frontiers Science Centre for Smart Materials Oriented Chemical Engineering, School of Bioengineering, Dalian University of Technology, Dalian 116024, China*

Chunxue Liu − *State Key Laboratory of Fine Chemicals, Frontiers Science Centre for Smart Materials Oriented Chemical Engineering, School of Bioengineering, Dalian University of Technology, Dalian 116024, China*

Bo Li − *Department of Mechanical Engineering, Kennesaw State University, Marietta, Georgia 30060, United States;* orcid.org/0000-0001-9407-9503

Ning Deng − *Department of Breast Surgery, Cancer Hospital of Dalian University of Technology, Liaoning Cancer Hospital and Institute, Shenyang 110042, China*

Complete contact information is available at: https://pubs.acs.org/10.1021/acs.nanolett.4c01693

Author Contributions

C. X. and W. K. conceived the project. W. K. designed the experiments. X. M., J. M., L. Y., J. L., W. L., C. L., and L. W. performed the experiments. W. K., B. L., and X. M. analyzed the data. X. M. wrote the manuscript, which was edited and approved by all authors. W. K. and C. X. helped summarize and give suggestions of the manuscript. X. M., L. Y., and J. L. contributed equally.

Notes

The authors declare no competing financial interest.

■ ACKNOWLEDGMENTS

Financial support for this work was provided via the National Key Research and Development Program (no.

2021YFC2103703), the National Natural Science Foundation (no. 22178046 and no. U22A20424), the Fundamental Research Funds for the Central Universities (no. LD2023026/DUT23YG110), and the Natural Science Foundation of Liaoning Province of China (2022-MS-129). We thank Dr. Zhiguang Sun and Dr. Hongbo Xie for AFM and TEM analysis. We acknowledge the assistance of DUT Core Facilities of the School of Bioengineering.

REFERENCES

(1) Aumiller, W. M.; Uchida, M.; Douglas, T. Protein cage assembly across multiple length scales. *Chem. Soc. Rev.* **2018**, *47* (10), 3433−3469.
(2) Edwardson, T. G. W.; Levasseur, M. D.; Tetter, S.; Steinauer, A.; Hori, M.; Hilvert, D. Protein Cages: From Fundamentals to Advanced Applications. *Chem. Rev.* **2022**, *122* (9), 9145−9197.
(3) Lucon, J.; Qazi, S.; Uchida, M.; Bedwell, G. J.; LaFrance, B.; Prevelige, J. P. E.; Douglas, T. Use of the interior cavity of the P22 capsid for site-specific initiation of atom-transfer radical polymerization with high-density cargo loading. *Nat. Chem.* **2012**, *4* (10), 781−788.
(4) Brasch, M.; Putri, R. M.; de Ruiter, M. V.; Luque, D.; Koay, M. S. T.; Castón, J. R.; Cornelissen, J. J. L. M. Assembling Enzymatic Cascade Pathways inside Virus-Based Nanocages Using Dual-Tasking Nucleic Acid Tags. *J. Am. Chem. Soc.* **2017**, *139* (4), 1512−1519.
(5) Edwardson, T. G. W.; Tetter, S.; Hilvert, D. Two-tier supramolecular encapsulation of small molecules in a protein cage. *Nat. Commun.* **2020**, *11* (1), 5410.
(6) Zhang, Y.; Feng, T.; Cao, Y.; Zhang, X.; Wang, T.; Huanca Nina, M. R.; Wang, L.; Yu, H.; Xu, J.; Ge, J.; Bai, Y. Confining Enzyme Clusters in Bacteriophage P22 Enhances Cofactor Recycling and Stereoselectivity for Chiral Alcohol Synthesis. *ACS Catal.* **2021**, *11* (16), 10487−10493.
(7) O'Neil, A.; Reichhardt, C.; Johnson, B.; Prevelige, P. E.; Douglas, T. Genetically Programmed In Vivo Packaging of Protein Cargo and Its Controlled Release from Bacteriophage P22. *Angew. Chem., Int. Ed.* **2011**, *50* (32), 7425−7428.
(8) Patterson, D. P.; Rynda-Apple, A.; Harmsen, A. L.; Harmsen, A. G.; Douglas, T. Biomimetic Antigenic Nanoparticles Elicit Controlled Protective Immune Response to Influenza. *ACS Nano* **2013**, *7* (4), 3036−3044.
(9) Uchida, M.; Kosuge, H.; Terashima, M.; Willits, D. A.; Liepold, L. O.; Young, M. J.; McConnell, M. V.; Douglas, T. Protein cage nanoparticles bearing the LyP-1 peptide for enhanced imaging of macrophage-rich vascular lesions. *ACS Nano* **2011**, *5* (4), 2493−2502.
(10) Uchida, M.; Flenniken, M. L.; Allen, M.; Willits, D. A.; Crowley, B. E.; Brumfield, S.; Willis, A. F.; Jackiw, L.; Jutila, M.; Young, M. J.; Douglas, T. Targeting of cancer cells with ferrimagnetic ferritin cage nanoparticles. *J. Am. Chem. Soc.* **2006**, *128* (51), 16626−16633.
(11) Lee, Y.; Kim, M.; Kang, J. Y.; Jung, Y. Protein Cages Engineered for Interaction-Driven Selective Encapsulation of Biomolecules. *ACS Appl. Mater. Interfaces* **2022**, *14* (31), 35357−35365.
(12) Moon, H.; Lee, J.; Min, J.; Kang, S. Developing Genetically Engineered Encapsulin Protein Cage Nanoparticles as a Targeted Delivery Nanoplatform. *Biomacromolecules* **2014**, *15* (10), 3794−3801.
(13) Edwardson, T. G. W.; Mori, T.; Hilvert, D. Rational Engineering of a Designed Protein Cage for siRNA Delivery. *J. Am. Chem. Soc.* **2018**, *140* (33), 10439−10442.
(14) Comellas-Aragones, M.; Engelkamp, H.; Claessen, V. I.; Sommerdijk, N. A.; Rowan, A. E.; Christianen, P. C.; Maan, J. C.; Verduin, B. J.; Cornelissen, J. J.; Nolte, R. J. A virus-based single-enzyme nanoreactor. *Nat. Nanotechnol.* **2007**, *2* (10), 635−639.
(15) Jenkins, M. C.; Lutz, S. Encapsulin Nanocontainers as Versatile Scaffolds for the Development of Artificial Metabolons. *ACS Synth. Biol.* **2021**, *10* (4), 857−869.
(16) Azuma, Y.; Zschoche, R.; Tinzl, M.; Hilvert, D. Quantitative Packaging of Active Enzymes into a Protein Cage. *Angew. Chem., Int. Ed.* **2016**, *55* (4), 1531−1534.
(17) Kang, W.; Ma, X.; Zhang, H.; Ma, J.; Liu, C.; Li, J.; Guo, H.; Wang, D.; Wang, R.; Li, B.; Xue, C. Dynamic Metabolons Using Stimuli-Responsive Protein Cages. *J. Am. Chem. Soc.* **2024**, *146* (10), 6686−6696.
(18) Patterson, D. P.; Prevelige, P. E.; Douglas, T. Nanoreactors by Programmed Enzyme Encapsulation Inside the Capsid of the Bacteriophage P22. *ACS Nano* **2012**, *6* (6), 5000−5009.
(19) Tan, T. K.; Rijal, P.; Rahikainen, R.; Keeble, A. H.; Schimanski, L.; Hussain, S.; Harvey, R.; Hayes, J. W. P.; Edwards, J. C.; McLean, R. K.; Martini, V.; Pedrera, M.; Thakur, N.; Conceicao, C.; Dietrich, I.; Shelton, H.; Ludi, A.; Wilsden, G.; Browning, C.; Zagrajek, A. K.; Bialy, D.; Bhat, S.; Stevenson-Leggett, P.; Hollinghurst, P.; Tully, M.; Moffat, K.; Chiu, C.; Waters, R.; Gray, A.; Azhar, M.; Mioulet, V.; Newman, J.; Asfor, A. S.; Burman, A.; Crossley, S.; Hammond, J. A.; Tchilian, E.; Charleston, B.; Bailey, D.; Tuthill, T. J.; Graham, S. P.; Duyvesteyn, H. M. E.; Malinauskas, T.; Huo, J.; Tree, J. A.; Buttigieg, K. R.; Owens, R. J.; Carroll, M. W.; Daniels, R. S.; McCauley, J. W.; Stuart, D. I.; Huang, K. A.; Howarth, M.; Townsend, A. R. A COVID-19 vaccine candidate using SpyCatcher multimerization of the SARS-CoV-2 spike protein receptor-binding domain induces potent neutralising antibody responses. *Nat. Commun.* **2021**, *12* (1), 542.
(20) Yenkoidiok-Douti, L.; Williams, A. E.; Canepa, G. E.; Molina-Cruz, A.; Barillas-Mury, C. Engineering a Virus-Like Particle as an Antigenic Platform for a Pfs47-Targeted Malaria Transmission-Blocking Vaccine. *Sci. Rep.* **2019**, *9* (1), 16833.
(21) Bruun, T. U. J.; Andersson, A. C.; Draper, S. J.; Howarth, M. Engineering a Rugged Nanoscaffold To Enhance Plug-and-Display Vaccination. *ACS Nano* **2018**, *12* (9), 8855−8866.
(22) Uchida, M.; McCoy, K.; Fukuto, M.; Yang, L.; Yoshimura, H.; Miettinen, H. M.; LaFrance, B.; Patterson, D. P.; Schwarz, B.; Karty, J. A.; Prevelige, P. E.; Lee, B.; Douglas, T. Modular Self-Assembly of Protein Cage Lattices for Multistep Catalysis. *ACS Nano* **2018**, *12* (2), 942−953.
(23) Oh, H. J.; Jung, Y. High order assembly of multiple protein cages with homogeneous sizes and shapes via limited cage surface engineering. *Chem. Sci.* **2023**, *14* (5), 1105−1113.
(24) Vervoort, D. F. M.; Heiringhoff, R.; Timmermans, S. B. P. E.; van Stevendaal, M. H. M. E.; van Hest, J. C. M. Dual Site-Selective Presentation of Functional Handles on Protein-Engineered Cowpea Chlorotic Mottle Virus-Like Particles. *Bioconjugate Chem.* **2021**, *32* (5), 958−963.
(25) Hess, G. T.; Cragnolini, J. J.; Popp, M. W.; Allen, M. A.; Dougan, S. K.; Spooner, E.; Ploegh, H. L.; Belcher, A. M.; Guimaraes, C. P. M13 bacteriophage display framework that allows sortase-mediated modification of surface-accessible phage proteins. *Bioconjugate Chem.* **2012**, *23* (7), 1478−1487.
(26) Kang, W.; Ma, X.; Kakarla, D.; Zhang, H.; Fang, Y.; Chen, B.; Zhu, K.; Zheng, D.; Wu, Z.; Li, B.; Xue, C. Organizing Enzymes on Self-Assembled Protein Cages for Cascade Reactions. *Angew. Chem., Int. Ed.* **2022**, *134* (52), No. e202214001.
(27) Zakeri, B.; Fierer, J. O.; Celik, E.; Chittock, E. C.; Schwarz-Linek, U.; Moy, V. T.; Howarth, M. Peptide tag forming a rapid covalent bond to a protein, through engineering a bacterial adhesin. *Proc. Natl. Acad. Sci. U.S.A.* **2012**, *109* (12), E690−E697.
(28) Keeble, A. H.; Yadav, V. K.; Ferla, M. P.; Bauer, C. C.; Chuntharpursat-Bon, E.; Huang, J.; Bon, R. S.; Howarth, M. DogCatcher allows loop-friendly protein-protein ligation. *Cell Chem. Biol.* **2022**, *29* (2), 339−350.
(29) Keeble, A. H.; Turkki, P.; Stokes, S.; Khairil Anuar, I. N. A.; Rahikainen, R.; Hytönen, V. P.; Howarth, M. Approaching infinite affinity through engineering of peptide-protein interaction. *Proc. Natl. Acad. Sci. U.S.A.* **2019**, *116* (52), 26523−26533.
(30) Szeto, T. H.; Rowland, S. L.; Habrukowich, C. L.; King, G. F. The MinD Membrane Targeting Sequence Is a Transplantable Lipid-binding Helix. *J. Biol. Chem.* **2003**, *278* (41), 40050−40056.

https://doi.org/10.1021/acs.nanolett.4c01693
Nano Lett. 2024, 24, 9237−9244

(31) Hu, Z.; Lutkenhaus, J. A conserved sequence at the C-terminus of MinD is required for binding to the membrane and targeting MinC to the septum. *Mol. Microbiol.* **2003**, *47* (2), 345−355.
(32) Thomik, T.; Wittig, I.; Choe, J.; Boles, E.; Oreb, M. An artificial transport metabolon facilitates improved substrate utilization in yeast. *Nat. Chem. Biol.* **2017**, *13* (11), 1158−1163.
(33) Li, X.; Jiang, Y.; Chong, S.; Walt, D. R. Bottom-up single-molecule strategy for understanding subunit function of tetrameric β-galactosidase. *Proc. Natl. Acad. Sci. U.S.A.* **2018**, *115* (33), 8346−8351.

https://doi.org/10.1021/acs.nanolett.4c01693
Nano Lett. 2024, 24, 9237−9244